
Inclusion of an inverse magnetic hysteresis model
into the space-time finite element method
for magnetoquasistatics

M. Gobrial, L. Domenig, M. Reichelt, M. Kaltenbacher, O. Steinbach

**Berichte aus dem
Institut für Angewandte Mathematik**

Technische Universität Graz

Inclusion of an inverse magnetic hysteresis model
into the space-time finite element method
for magnetoquasistatics

M. Gobrial, L. Domenig, M. Reichelt, M. Kaltenbacher, O. Steinbach

**Berichte aus dem
Institut für Angewandte Mathematik**

Bericht 2025/2

Technische Universität Graz
Institut für Angewandte Mathematik
Steyrergasse 30
A 8010 Graz

WWW: <http://www.applied.math.tugraz.at>

© Alle Rechte vorbehalten. Nachdruck nur mit Genehmigung des Autors.

INCLUSION OF AN INVERSE MAGNETIC HYSTERESIS MODEL INTO THE SPACE-TIME FINITE ELEMENT METHOD FOR MAGNETOQUASISTATICS

M. GOBRIAL¹, L. DOMENIG², M. REICHEL¹,
M. KALTENBACHER², O. STEINBACH¹

¹*Institute of Applied Mathematics, TU Graz, Austria*

²*Institute of Fundamentals and Theory in Electrical Engineering, TU Graz, Austria*

ABSTRACT. In this note we discuss the numerical solution of the eddy current approximation of the Maxwell equations using the simple Pragmatic Algebraic Model to include hysteresis effects. In addition to the more standard time-stepping approach we propose a space-time finite element method which allows both for parallelization and adaptivity simultaneously in space and time. Numerical experiments confirm both approaches yield the same numerical results.

Keywords: Nonlinear magnetoquasistatics, finite-elements, iterative solvers, Newton method, space-time, hysteresis

1. INTRODUCTION

For the mathematical modeling of the electromagnetic behavior in an electric machine, e.g. an electric motor or a transformer, we consider the eddy current approximation of Maxwell's equations in the low-frequency regime, cf., e.g., [1, 2, 3],

$$\operatorname{curl} \mathbf{H} = \mathbf{j}_s, \quad \operatorname{div} \mathbf{B} = 0, \quad \operatorname{curl} \mathbf{E} = -\partial_t \mathbf{B} \quad \text{in } D \subset \mathbb{R}^3, \quad (1)$$

with boundary conditions $\mathbf{B} \cdot \mathbf{n} = 0$ on ∂D . For simplicity we consider a fixed domain D , for which we can write Ohm's law as $\mathbf{J} = \sigma \mathbf{E}$; for the case of a moving domain, see, e.g., [4]. In addition to the Maxwell equations (1) we need to have a constitutive relation $\mathbf{H} = \mathbf{H}(\mathbf{B})$ which in many cases is described in terms of the magnetic reluctivity ν and, in presence of permanent magnets, the permanent magnetization \mathbf{M} , i.e.

$$\mathbf{H} = \nu(\|\mathbf{B}\|) \mathbf{B} - \mathbf{M}. \quad (2)$$

Note that ν may depend on the magnitude of the magnetic flux density \mathbf{B} as e.g. for ferromagnetic materials, see, e.g., [5]. Although the constitutive law (2) covers a wide range of physically relevant phenomena, it neglects the effects of hysteresis. These effects become more and more important to accurately describe electrical devices, such as electric machines and transformers. For this reason, it is necessary to employ material models that cover hysteresis

into the mathematical model, and its numerical simulation by finite element methods. For the standard finite element method, this has already successfully been done in the static case using the magnetic scalar potential [6] as well as using the magnetic vector potential [7]. For transient simulations, there exist also approaches to consider the hysteresis effect in the finite element method using a magnetic vector potential [8, 9]. To the authors knowledge, however, there exists no approach to incorporate hysteretic material models into a space-time finite element framework.

Since the magnetic flux density is a solenoidal vector field, $\mathbf{B} = \text{curl } \mathbf{A}$, we can rewrite the eddy current problem (1) in its equivalent vector potential formulation [3, 10]

$$\sigma \partial_t \mathbf{A} + \text{curl}[\nu \text{curl } \mathbf{A}] = \mathbf{j}_s + \text{curl } \mathbf{M}, \quad (3)$$

where we have used the constitutive law (2). Usually, gauging techniques are applied in order to ensure the uniqueness of the vector potential \mathbf{A} , see, e.g., [10, 11]. A common simplification of the eddy current problem (3) is the reduction to a two-dimensional model problem assuming that one dimension of the computational domain is much larger than the other dimensions and that the geometry is invariant in the larger scale, cf. [12]. Hence, we can pose the eddy current problem on a cross section $\Omega \subset \mathbb{R}^2$ of the electric machine in D , where the electromagnetic quantities take the form

$$\mathbf{H} = \begin{pmatrix} H_1(x_1, x_2, t) \\ H_2(x_1, x_2, t) \\ 0 \end{pmatrix}, \quad \mathbf{M} = \begin{pmatrix} M_1(x_1, x_2, t) \\ M_2(x_1, x_2, t) \\ 0 \end{pmatrix}, \quad \mathbf{j}_s = \begin{pmatrix} 0 \\ 0 \\ j_s(x_1, x_2, t) \end{pmatrix}.$$

It follows that \mathbf{j}_s is divergence free by construction, and the magnetic flux density \mathbf{B} must admit the same form as the electric field intensity \mathbf{H} , due to (2). Using $\mathbf{B} = \text{curl } \mathbf{A}$ we further have

$$\mathbf{A} = \begin{pmatrix} 0 \\ 0 \\ u(x_1, x_2, t) \end{pmatrix}, \quad \mathbf{B} = \begin{pmatrix} \partial_{x_2} u(x_1, x_2, t) \\ -\partial_{x_1} u(x_1, x_2, t) \\ 0 \end{pmatrix}. \quad (4)$$

With this we can rewrite (3) for $(x, t) \in Q := \Omega \times (0, T)$ as

$$\sigma(x) \partial_t u(x, t) - \text{div}_x [\nu(x, |u|) \nabla_x u(x, t)] = j_s(x, t) - \text{div}_x M^\perp(x, t), \quad (5)$$

where $M^\perp = (-M_2, M_1)^\top$ is the perpendicular of the magnetization and $T > 0$ is the final time. For the sake of completeness, boundary conditions $u = 0$ on $\Sigma := \partial\Omega \times (0, T)$ as well as an initial condition $u(0) = 0$ in Ω must be set. Although, this approach (5) of the eddy current problem is indeed a typical approximation in the context of electric machines, it does not consider hysteresis effects. In this work, we will apply a specific law among many, that considers the effect of hysteresis in terms of the constitutive law (2).

The remainder of this work is organized as follows. In Section 2 we introduce the Pragmatic Algebraic Model (PAM), a specific vector hysteresis model previously analyzed in [7, 9, 13]. We incorporate this constitutive law into Maxwell's equations (1) and formulate the problem on the cross section Ω of the geometry

D to derive the underlying parabolic evolution problem (8). Section 3 presents two numerical approaches for solving the resulting time-dependent partial differential equation. On the one hand, we formulate a classical time stepping method [14], and on the other hand, we describe a space-time finite element method motivated by [15]. A comparative analysis of both is provided in Section 4, indicating a good agreement of the results.

2. HYSTERESIS MODEL

The aim of this section is to modify the eddy current problem (5) to a model, which can consider hysteresis effects. A physical system subject to hysteresis does not only depend on the input data but also on the history of these data [16]. For ferromagnetic materials, e.g., iron, hysteresis effects are quite natural and shall be considered in the constitutive law.

In this work we consider the Pragmatic Algebraic Model (PAM) as hysteresis model, which uses six real positive parameters $p_j \in \mathbb{R}_+$, $j = 0, \dots, 5$, in one algebraic expression in order to describe hysteresis, see [17]. In contrast to other hysteresis models, the efficiency of PAM lies in its formulation by one algebraic expression, which takes the static and the dynamic effects into account. The adapted constitutive law reads as

$$\mathbf{H} = f(\mathbf{B})\mathbf{B} + g(\partial_t\mathbf{B})\partial_t\mathbf{B} - \mathbf{M}, \quad (6)$$

where

$$f(\mathbf{B}) = p_0 + p_1\|\mathbf{B}\|^{2p_2}, \quad g(\partial_t\mathbf{B}) = p_3 + \frac{p_4}{\sqrt{p_5^2 + \|\partial_t\mathbf{B}\|^2}}.$$

The first expression $f(\mathbf{B})$ of (6) describes the anhysteretic part, which is in fact similar to the magnetic reluctivity ν , which reflects the BH-curve relation described by (2). The parameters p_0, p_1, p_2 can be fitted in order to obtain the same behavior as ν in the classical approach. The second expression $g(\partial_t\mathbf{B})$ describes on one hand the macroscopic eddy currents by the parameter p_3 , and on the other hand the hysteresis effects, that are considered by p_4 and p_5 , cf. [17]. As before, \mathbf{M} is the permanent magnetization of occurring permanent magnets. Now, when using the constitutive law (6) instead of (2) and again the vector potential $\mathbf{B} = \text{curl } \mathbf{A}$, the underlying eddy current equation considering hysteresis reads as

$$\sigma\partial_t\mathbf{A} + \text{curl} \left(f(\text{curl}(\mathbf{A})) \text{curl}(\mathbf{A}) + g(\text{curl}(\partial_t\mathbf{A})) \text{curl}(\partial_t\mathbf{A}) \right) = \mathbf{j}_s + \text{curl}(\mathbf{M}). \quad (7)$$

The reduction to the spatially two-dimensional case requires the same assumptions as above, hence the vector potential \mathbf{A} has the same form as in (4), and we can rewrite (7) as

$$\sigma\partial_t u - \text{div}_x [f(|\nabla_x u|)\nabla_x u + g(|\partial_t \nabla_x u|)\partial_t \nabla_x u] = j_s - \text{div}_x M^\perp \quad (8)$$

in $Q := \Omega \times (0, T)$. In addition to the partial differential equation (8) we consider homogeneous Dirichlet boundary conditions $u = 0$ on $\Sigma := \partial\Omega \times (0, T)$, which implies the induction boundary condition $B \cdot n = 0$, and the initial condition $u(x, 0) = 0$ for $x \in \Omega$.

3. FINITE ELEMENT FORMULATION

3.1. Time Stepping Framework. When multiplying the time dependent partial differential equation (8) with a spatial test function v vanishing on $\partial\Omega$, integrating over Ω and applying integration by parts, we obtain

$$\begin{aligned} \int_{\Omega} \sigma \partial_t u v \, dx + \int_{\Omega} \left[f(|\nabla_x u|) \nabla_x u + g(|\partial_t \nabla_x u|) \partial_t \nabla_x u \right] \cdot \nabla_x v \, dx \\ = \int_{\Omega} \left[j_s v + M^\perp \cdot \nabla_x v \right] \, dx. \end{aligned} \quad (9)$$

Let $S_h^1(\Omega) = \text{span}\{\phi_k\}_{k=1}^{M_\Omega}$ be the standard finite element space of piecewise linear basis functions ϕ_k which are defined with respect to an admissible decomposition of the computational domain Ω into shape regular triangular finite elements τ_ℓ of the spatial mesh size h_x , $\ell = 1, \dots, N_\Omega$, and which are zero on $\partial\Omega$. The semi-discretization of (9) is then equivalent of a system of nonlinear ordinary differential equations,

$$[M_h + A_h(\dot{u}_h)]\dot{\underline{u}}(t) + K_h(u_h)\underline{u}(t) = \underline{F}(t), \quad (10)$$

where the entries of the mass and stiffness matrices as well as of the load vector are given by, for $j, k = 1, \dots, M_\Omega$,

$$\begin{aligned} M_h[j, k] &= \int_{\Omega} \sigma(x) \phi_k(x) \phi_j(x) \, dx, \\ K_h(u_h)[j, k] &= \int_{\Omega} f(|\nabla_x u_h(x, t)|) \nabla_x \phi_k(x) \cdot \nabla_x \phi_j(x) \, dx, \\ A_h(\dot{u}_h)[j, k] &= \int_{\Omega} g(|\nabla_x \dot{u}_h(x, t)|) \partial_t \nabla_x \phi_k(x) \cdot \nabla_x \phi_j(x) \, dx, \\ F_j(t) &= \int_{\Omega} \left[j_s(x, t) \phi_j(x) + M^\perp(x, t) \cdot \nabla_x \phi_j(x) \right] \, dx. \end{aligned}$$

Note that $\underline{u}(t) \in \mathbb{R}^{M_\Omega}$ is the vector of the time dependent coefficients of the numerical solution

$$u_h(x, t) = \sum_{k=1}^{M_\Omega} u_k(t) \phi_k(x).$$

For time discretization we introduce a temporal mesh size h_t and we define time steps $t_i = ih_i$, $i = 0, \dots, N_T$. When considering

$$u_h(x, t_i) = \sum_{k=1}^{M_\Omega} u_k(t_i) \phi_k(x) = \sum_{k=1}^{M_\Omega} u_k^i \phi_k(x) = u_h^i(x),$$

and using the backward finite difference scheme

$$\dot{u}_h(x, t_i) \simeq \frac{1}{h_t} [u_h(x, t_i) - u_h(x, t_{i-1})] = \frac{1}{h_t} \sum_{k=1}^{M_\Omega} [u_k^i - u_k^{i-1}] \phi_k(x),$$

the time discretization of (10) results in a sequence of nonlinear systems of algebraic equations, $i = 1, \dots, N_T$,

$$\frac{1}{h_t} [M_h + A_h((u_h^i - u_h^{i-1})/h_t)] [\underline{u}^i - \underline{u}^{i-1}] + K_h(u_h^i) \underline{u}^i(t) = \underline{F}(t_i), \quad (11)$$

with the initial condition $\underline{u}^0 = \underline{0}$. At each time step t_i , $i = 1, \dots, N_T$, the nonlinear system (11) is solved via Newton's method where we use the results as given in [9] to compute all involved derivatives analytically.

3.2. Space-Time Framework. Next we consider a space-time variational formulation for the eddy current problem(8). We now multiply the transient partial differential equation (8) with a test function $v(x, t)$ vanishing on $\Sigma = \partial\Omega \times (0, T)$, and integrate over the space-time domain $Q = \Omega \times (0, T)$. Integration by parts only with respect to the spatial components finally provides the space-time variational formulation

$$\begin{aligned} & \int_0^T \int_{\Omega} \sigma \partial_t u v \, dx \, dt + \int_0^T \int_{\Omega} f(|\nabla_x u|) \nabla_x u \cdot \nabla_x v \, dx \, dt \\ & + \int_0^T \int_{\Omega} g(|\partial_t \nabla_x u|) \partial_t \nabla_x u \cdot \nabla_x v \, dx \, dt = \int_0^T \int_{\Omega} [j_s v + M^\perp \cdot \nabla_x v] \, dx \, dt. \end{aligned} \quad (12)$$

Let $S_h^1(Q) = \text{span}\{\varphi_k\}_{k=1}^{M_Q}$ be the space-time finite element space of piecewise linear basis functions φ_k which are defined with respect to an admissible decomposition of the space-time domain Q into tetrahedral finite elements q_ℓ , $\ell = 1, \dots, N_Q$ of mesh size h , and which are zero at initial time $t = 0$, and on the lateral boundary Σ . However, since second order derivatives occur in the weak formulation (12), we can not use $S_h^1(Q)$ for a conforming finite element discretization of (12). Instead, we use the substitution $p(x, t) := \partial_t u(x, t)$ to rewrite (12) as

$$\begin{aligned} & \int_0^T \int_{\Omega} \sigma \partial_t u v \, dx \, dt + \int_0^T \int_{\Omega} f(|\nabla_x u|) \nabla_x u \cdot \nabla_x v \, dx \, dt \\ & + \int_0^T \int_{\Omega} g(|\nabla_x p|) \nabla_x p \cdot \nabla_x v \, dx \, dt = \int_0^T \int_{\Omega} [j_s v + M^\perp \cdot \nabla_x v] \, dx \, dt, \end{aligned} \quad (13)$$

together with a second variational formulation

$$\int_0^T \int_{\Omega} p(x, t) q(x, t) \, dx \, dt = \int_0^T \int_{\Omega} \partial_t u(x, t) q(x, t) \, dx \, dt. \quad (14)$$

Since $p = \partial_t u$ only has zero boundary conditions on Σ , there are no initial conditions at $t = 0$. For the space-time finite element approximation of p we therefore have to use the extended finite element space $\widetilde{S}_h^1(Q) = \text{span}\{\varphi_k\}_{k=1}^{\widetilde{M}_Q}$, where the additional basis functions φ_k , $k = M_Q + 1, \dots, \widetilde{M}_Q$ are related to the nodes at $t = 0$. The space-time finite element discretization of the system (13) and (14) is then equivalent to a system of nonlinear algebraic equations,

$$\begin{pmatrix} B_h + K_h(u_h) & A_h(p_h) \\ -\widetilde{B}_h & M_h \end{pmatrix} \begin{pmatrix} \underline{u} \\ \underline{p} \end{pmatrix} = \begin{pmatrix} \underline{F} \\ \underline{0} \end{pmatrix}, \quad (15)$$

where the entries of the block matrices are given by, for $k, \ell = 1, \dots, M_Q$ and $i, j = 1, \dots, \widetilde{M}_Q$,

$$\begin{aligned} B_h[\ell, k] &= \int_0^T \int_{\Omega} \sigma(x) \partial_t \varphi_k(x, t) \varphi_{\ell}(x, t) dx dt, \\ K_h(u_h)[\ell, k] &= \int_0^T \int_{\Omega} f(|\nabla_x u_h(x, t)|) \nabla_x \varphi_k(x, t) \cdot \varphi_{\ell}(x, t) dx dt, \\ A_h(p_h)[\ell, i] &= \int_0^T \int_{\Omega} g(|\nabla_x p_h|) \nabla_x \varphi_i(x, t) \cdot \nabla_x \varphi_{\ell}(x, t) dx dt, \\ M_h[j, i] &= \int_0^T \int_{\Omega} \varphi_i(x, t) \cdot \varphi_j(x, t) dx dt, \\ \widetilde{B}_h[j, k] &= \int_0^T \int_{\Omega} \partial_t \varphi_k(x, t) \varphi_j(x, t) dx dt. \end{aligned}$$

In addition, the entries of the load vector are given as

$$F_{\ell} = \int_0^T \int_{\Omega} \left[j_s(x, t) \varphi_{\ell}(x, t) + M^{\perp}(x, t) \cdot \nabla_x \varphi_{\ell}(x, t) \right] dx dt, \quad \ell = 1, \dots, M_Q,$$

and $\underline{u} \in \mathbb{R}^{M_Q}$ and $\underline{p} \in \mathbb{R}^{\widetilde{M}_Q}$ are the coefficient vectors of the finite element functions u_h and p_h , respectively. Since the space-time mass matrix M_h is invertible, we can compute $\underline{p} = M_h^{-1} \widetilde{B}_h \underline{u} \leftrightarrow p_h$ to conclude the nonlinear Schur complement system

$$\left[B_h + K_h(u_h) + A_h(p_h) M_h^{-1} \widetilde{B}_h \right] \underline{u} = \underline{F}. \quad (16)$$

To solve the global nonlinear system (16), we use an exact Newton method with Armijo's damping strategy [18], where the linearized system of each Newton iteration is solved with the parallel direct solver MUMPS supported by PETCs [19], which is based on a mesh decomposition method provided by the finite element library Netgen/NGSolve [20].

4. NUMERICAL RESULTS

In this section we want to compare the proposed methods. While the space-time formulation (16) has to deal with a three-dimensional problem, which is further blown up to a system for the additional variable p_h , the time-stepping method simply considers the two-dimensional spatial problem. However, the large system of the space-time method needs to be solved in parallel only once, whereas the time-stepping method needs to solve the spatial problem sequentially for each time step. The upcoming examples will first give a comparison between these two methods with respect to an academic model problem. Secondly, the Team problem 32 [21] will be considered, which verifies the applicability of the proposed hysteresis problem (6) as well as the accuracy of the introduced methods for solving the eddy current equation including hysteresis.

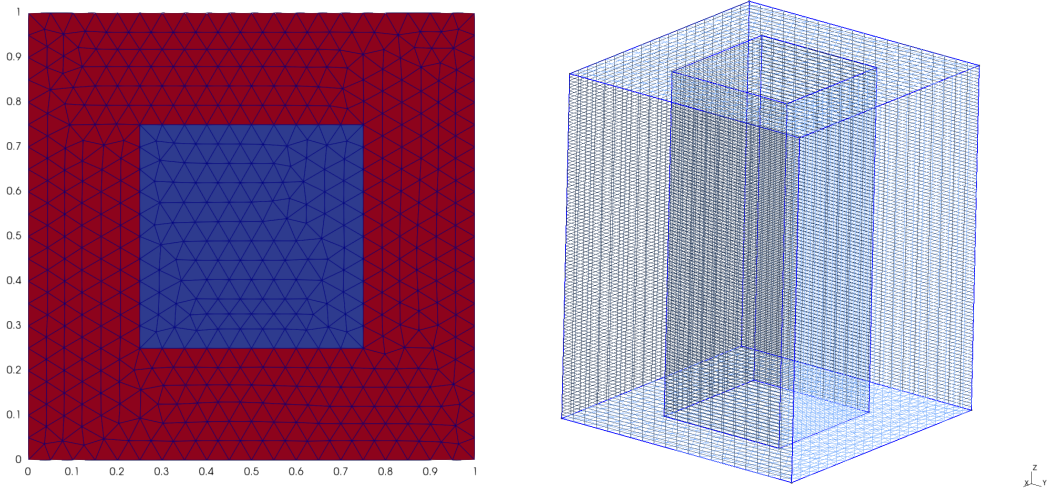


FIGURE 1. Left: The domain $\Omega = (0, 1)^2$ consisting of two materials Ω_{cu} (in blue) and Ω_{fe} (in red). Right: The space-time mesh $Q = \Omega \times (0, T)$, which has 100 time slices in temporal direction, 53.530 nodes and 293.400 elements.

4.1. Simple Geometry. The first example considers a two-dimensional spatial domain $\Omega = (0, 1)^2$, which consists of two different materials, $\Omega_{cu} = (0, 25, 0.75)^2$ consisting of copper through which the excitation j_s passes, and $\Omega_{fe} = \Omega \setminus \Omega_{cu}$ consisting of iron in which the hysteresis model is obtained. The final time is given as $T = 1.25$. Figure 1 shows the spatial domain, as well as the structured space-time mesh for the space-time finite element method. Furthermore, we use the following parameters,

$$\sigma(x) = \begin{cases} 0 & \text{in } \Omega_{cu}, \\ 0.01 & \text{in } \Omega_{fe}, \end{cases} \quad f(|\nabla_x u|) = \begin{cases} \frac{10^7}{4\pi} & \text{in } \Omega_{cu}, \\ p_0 + p_1 |\nabla_x u|^{2p_2} & \text{in } \Omega_{fe}, \end{cases}$$

$$j_s(x, t) = \begin{cases} 2000 \sin(2\pi t) & \text{in } \Omega_{cu}, \\ 0 & \text{in } \Omega_{fe}, \end{cases} \quad g(|\partial_t \nabla_x u|) = \begin{cases} 0 & \text{in } \Omega_{cu}, \\ p_3 + \frac{p_4}{\sqrt{p_5^2 + |\partial_t \nabla_x u|^2}} & \text{in } \Omega_{fe}, \end{cases}$$

where $p_0 = 75.6$, $p_1 = 0.0223$, $p_2 = 11.47$, $p_3 = 0.0001$, $p_4 = 65.8$, $p_5 = 1$. Note that, the equivalence $g(|\nabla_x p|) = g(|\partial_t \nabla_x u|)$ holds on the continuous level, and that $M^\perp = (0, 0)^\top$, since no permanent magnets occur. Figure 2 visualizes the magnetic flux density \mathbf{B}_x (in the x-component) as well as the hysteresis curve and yields that both methods produce almost the same results.

4.2. Two-Phase Transformer – TEAM Problem 32. Our second example is a two-phase transformer given by the TEAM problem 32 [21], which presents the electric field simulation including hysteresis on a three limbed ferromagnetic core with two thin windings, see Figure 3. The two-dimensional computational domain Ω has the same dimensions as in [21] and consists of three different materials, the iron core Ω_{fe} , the windings Ω_{cu} at the external limbs and air Ω_a .

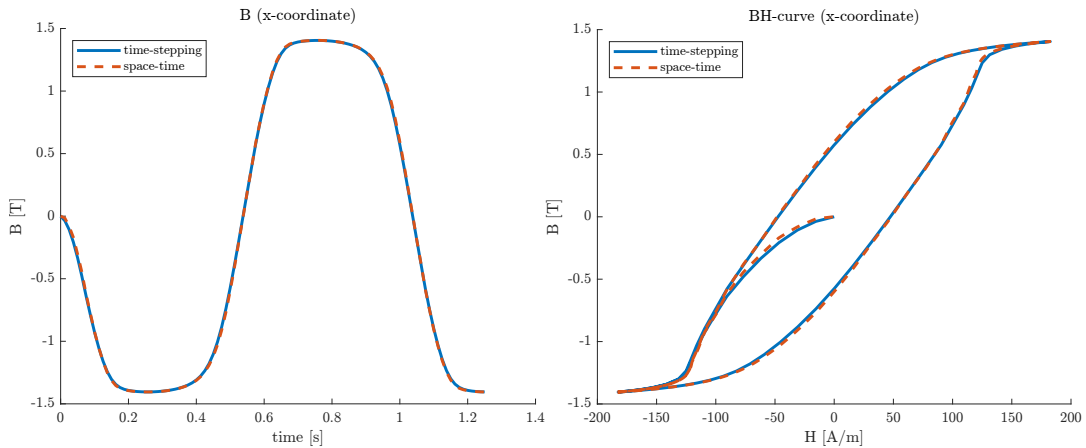


FIGURE 2. Left: The magnetic flux density B_x over time. Right: The BH-curve indicating the hysteresis effect.

The considered time span is for $T = 0.1$ and the parameters are

$$\sigma(x) = \begin{cases} 0 & \text{in } \Omega_{cu} \cup \Omega_a, \\ 0 & \text{in } \Omega_{fe}, \end{cases} \quad f(|\nabla_x u|) = \begin{cases} \frac{10^7}{4\pi} & \text{in } \Omega_{cu} \cup \Omega_a \\ p_0 + p_1 |\nabla_x u|^{2p_2} & \text{in } \Omega_{fe}, \end{cases}$$

$$j_s(x, t) = \begin{cases} \tilde{j}(t) & \text{in } \Omega_{cu}, \\ 0 & \text{in } \Omega_{fe} \cup \Omega_a, \end{cases} \quad g(|\partial_t \nabla_x u|) = \begin{cases} 0 & \text{in } \Omega_{cu} \cup \Omega_a \\ p_3 + \frac{p_4}{\sqrt{p_5^2 + |\partial_t \nabla_x u|^2}} & \text{in } \Omega_{fe}, \end{cases}$$

where $p_0 = 181,88232$, $p_1 = 0.267053$, $p_2 = 8.999565$, $p_3 = 0.00001$, $p_4 = 0.0001$, $p_5 = 50$ and the current density \tilde{j} is a B-spline interpolation of the measured current values from [21] multiplied with 90, the number of turns, and divided by the area of the winding, cf. Figure 5. Since no permanent magnets occur, we have $M^\perp = (0, 0)^\top$. Figure 4 depicts the magnetic flux density \mathbf{B}_y (in the y-component), which shows, that both methods agree well. It also visualizes the BH-curve, in which the hysteresis effect is visible and both methods indicate this behavior very well.

5. CONCLUSION

In this paper, we have formulated the eddy current approximation derived from Maxwell's equations in the low-frequency regime, incorporating a specific hysteresis model for the numerical simulation of electromagnetic fields. The nonlinear hysteresis model PAM is represented by a single algebraic expression, making it an efficient choice for capturing hysteresis effects. To solve the resulting nonlinear time-dependent PDE, we employed two different numerical approaches. The first is a classical semi-discretization method, where the finite element method is used for spatial discretization, followed by an implicit time-stepping scheme. The second approach is a space-time finite element method, which requires solving a saddle-point system but allows the entire problem to be solved at once, enabling parallel computations in spatial and temporal directions simultaneously. Finally, we compared both methods and demonstrated

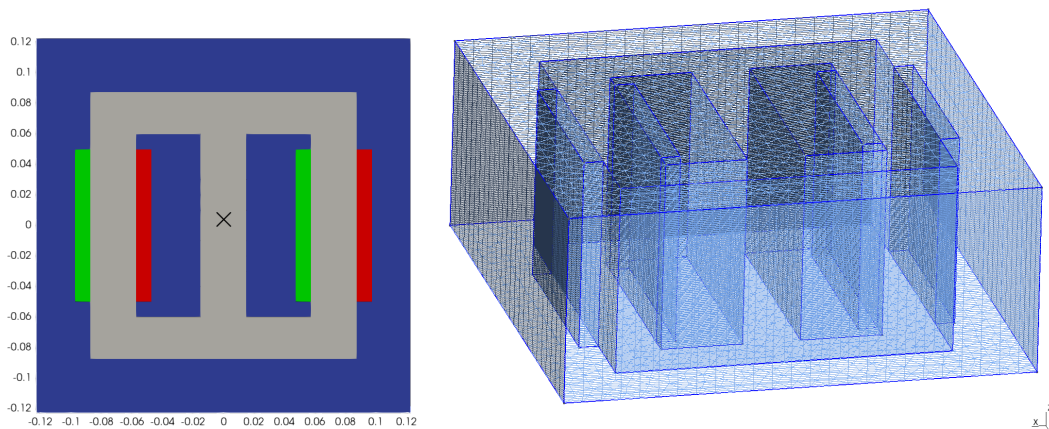


FIGURE 3. Left: The domain Ω of the transformer consisting of the iron core Ω_{fe} (in gray), the windings Ω_{cu} (in green and red) and air Ω_a (in blue). Right: The space-time mesh $Q = \Omega \times (0, T)$, which has 100 time slices in temporal direction, 91.405 nodes and 206856 elements.

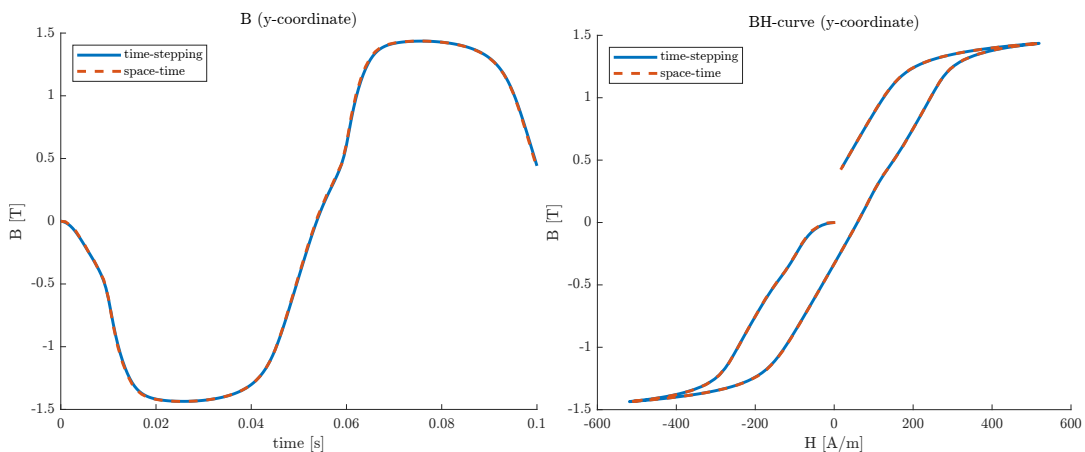


FIGURE 4. Left: The magnetic flux density B_x over time. Right: The BH-curve indicating the hysteresis effect.

the applicability of the hysteresis model by achieving similar simulation results. However, the main advantage of space-time finite element methods is the possibility to use adaptivity simultaneously in space and time in order to resolve the potential u locally, and therefore reduce the total number of degrees of freedom to reach a prescribed accuracy. A more detailed numerical analysis of such an adaptive space-time finite element approach will be done in future research.

Acknowledgements. This work was supported by the joint DFG/FWF Collaborative Research Centre CREATOR (DFG: Project-ID 492661287/TRR 361; FWF: 10.55776/F90) at TU Darmstadt, TU Graz and JKU Linz.

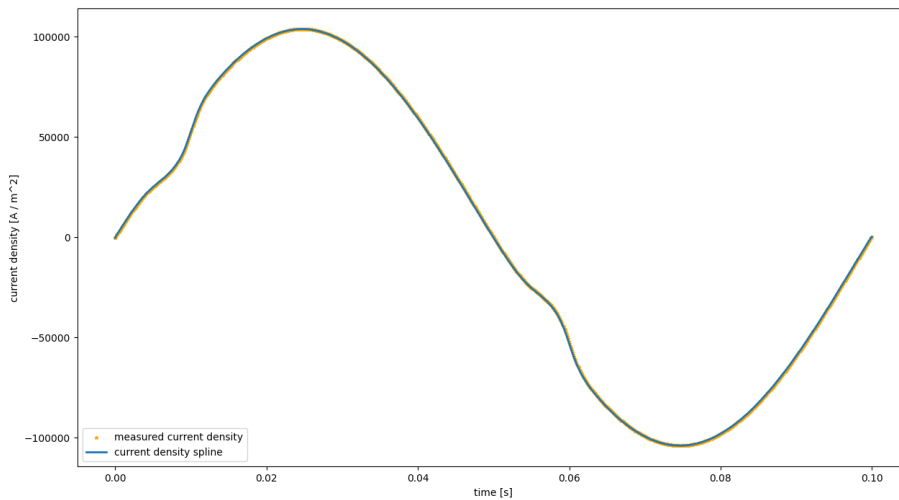


FIGURE 5. The current density spline \tilde{j} (in blue) interpolated with respect to the measured values (in orange) of test case 1A from [21].

REFERENCES

- [1] A. Alonso Rodríguez and A. Valli, *Eddy Current Approximation of Maxwell Equations: Theory, Algorithms and Applications*. Milano: Springer, 2010.
- [2] J. Jackson, *Classical Electrodynamics*. Wiley, 1999.
- [3] P. Monk, *Finite Element Methods for Maxwell's Equations*. Oxford Academic, 2003.
- [4] P. Gangl, M. Gobrial, and O. Steinbach, "A space-time finite element method for the eddy current approximation of rotating electric machines," *Comput. Methods Appl. Math.*, vol. 25, pp. 441–457, 2025.
- [5] G. Meunier, *The Finite Element Method for Electromagnetic Modeling*. Wiley, 2008.
- [6] L. D. Domenig, K. Roppert, and M. Kaltenbacher, "Incorporation of a 3-d energy-based vector hysteresis model into the finite element method using a reduced scalar potential formulation," *IEEE Trans. Magn.*, vol. 60, no. 6, pp. 1–8, 2024.
- [7] X. Xiao, F. Müller, M. M. Nell, and K. Hameyer, "Modeling anisotropic magnetic hysteresis properties with vector stop model by using finite element method," *COMPEL*, vol. 41, no. 2, pp. 752–763, 2022.
- [8] K. Jacques, *Energy-Based Magnetic Hysteresis Models - Theoretical Development and Finite Element Formulations*. PhD thesis, Université de Liège, 2018.
- [9] F. Purnode, F. Henrotte, G. Louppe, and C. Geuzaine, "Neural network-based simulation of fields and losses in electrical machines with ferromagnetic laminated cores," *Int. J. Numer. Model.*, vol. 37, no. 2, p. e3226, 2024.
- [10] M. Kaltenbacher, *Numerical Simulation of Mechatronic Sensors and Actuators*. Berlin, Heidelberg: Springer, 2015.
- [11] C. Hafner, *Numerische Berechnung elektromagnetischer Felder*. Berlin: Springer, 1987.
- [12] S. Clain, J. Rappaz, M. Swierkosz, and R. Touzani, "Numerical modeling of induction heating for two-dimensional geometries," *Math. Models Methods Appl. Sci.*, vol. 3, no. 6, pp. 805–822, 1993.

- [13] F. Henrotte, S. Steentjes, K. Hameyer, and C. Geuzaine, “Pragmatic two-step homogenisation technique for ferromagnetic laminated cores,” *IET Sci. Meas. Technol.*, vol. 9, no. 2, pp. 152–159, 2015.
- [14] V. Thomée, *Galerkin finite element methods for parabolic problems*, vol. 25 of *Springer Series in Computational Mathematics*. Berlin: Springer, 2006.
- [15] O. Steinbach, “Space-time finite element methods for parabolic problems,” *Comput. Methods Appl. Math.*, vol. 15, no. 4, pp. 551–566, 2015.
- [16] M. Brokate and J. Sprekels, *Hysteresis and Phase Transitions*. Applied Mathematical Sciences, New York: Springer, 1996.
- [17] X. Xiao, F. Müller, G. Bavendiek, and K. Hameyer, “Analysis of vector hysteresis models in comparison to anhysteretic magnetization model,” *Eur. Phys. J. Appl. Phys.*, vol. 91, no. 2, p. 20901, 2020.
- [18] P. Deuffhard, *Newton Methods for Nonlinear Problems: Affine Invariance and Adaptive Algorithms*. Springer Series in Computational Mathematics, Springer, 2011.
- [19] L. D. Dalcin, R. R. Paz, P. A. Kler, and A. Cosimo, “Parallel distributed computing using Python,” *Adv. Water Resour.*, vol. 34, no. 9, pp. 1124–1139, 2011.
- [20] J. Schöberl, “NETGEN: An advancing front 2d/3d-mesh generator based on abstract rules,” *Comput. Visual. Sci.*, vol. 1, pp. 41–52, 1997.
- [21] O. Bottauscio, M. Chiampi, C. Ragusa, L. Rege, and M. Repetto, “A test case for validation of magnetic field analysis with vector hysteresis,” *IEEE Trans. Magn.*, vol. 38, pp. 893–896, 2002.